*Russian Journal of General Chemistry, Vol. 72, No. 4, 2002, pp. 642–656. Translated from Zhurnal Obshchei Khimii, Vol. 72, No. 4, 2002, pp. 688–703.*


# Photochemical Method of Controlling Dispersity of Nanostructures of Transition Metals

**T. B. Boitsova, V. V. Gorbunova, and E. I. Volkova**

*Gertsen Russian State Pedagogical University, St. Petersburg, Russia*

Received November 5, 2001

**Abstract** — Original methods of photochemical preparation of stable mono- (Cu, Ag, Au, Ni, Pd, Pt) and bimetallic nanoparticles in the form of optically transparent compact films on quartz surface and of volume dispersions in porous inorganic (silica glasses) and organic (MF-4SK fluorocarbon) materials, solid polymers (polyvinyl alcohol, polyethylene glycol, gelatin, latexes), and in liquid media (glycerol) are reviewed. The results of studies of spectral and structural characteristics of nanophase films under various experimental conditions are presented. Experimental mechanistic models and ways of controlling disperse composition of metal colloids, which can be used for photochemical synthesis of nanophase systems, are proposed.

Deposition of colloidal forms of metals on dielectric surfaces and in bulk solutions is a topical question of producing functional nanophase materials and supported catalysts. The wide application of materials on the basis of colloidal metals is caused by the unique combination of electrical, magnetic, optical, catalytic, and other properties of these particles, atypical of bulk metals. Colloidal metals deposited on solid surfaces are widely used in creating materials for electronics and laser optics, in developing techniques for absorption and emission spectroscopy, and in military industry. Colloids precipitated in polymeric matrices are used for creating anticorrosive coatings. The application of metallic colloids (of silver) in production of bioactive preparations has also been reported.

In the last few years, bimetallic colloids are gaining ground due to the unique possibility of varying their donor–acceptor properties. To date, the problem is that these reactive species whose properties are strongly dependent on dimensions, composition, and surface admixtures are difficult to prepare. The existing methods of preparation of nanometals fail to ensure necessary reproducibility or are too expensive for wide usage. Therefore, search for an accessible reproducible method of synthesis is a high-priority fundamental problem.

As follows from an analysis of practically useful properties of materials on the basis of metal colloids, the method for preparing the colloids should satisfy certain requirements: It should reliably secure the necessary particle size and high size uniformity (high monodispersity) of the resulting samples and provide reproducible results. Comparison of various methods showed that these requirements are satisfied by the photochemical method [1–6]. The advantages of the photochemical method are: (a) high simplicity and low cost of equipment; (b) high "purity" of the reducing agent used (light quanta) which is able to reduce many transition metal ions fast and effectively; and (c) good reproducibility in a wide temperature range and in various media. Importantly, the photosynthetic process does not require deaeration and use of stabilizers which are powerful catalytic poisons (surfactants, micelles, π-acceptor ligands). As compared with colloids obtained traditionally (chemical reduction, high-frequency discharge, ultrasonic dispergation, metal vapor deposition), photosynthesized colloids are distinguished by narrow size distribution (high monodispersity) and high stability. The copper, silver, and gold colloids we synthesized at our laboratory in porous glasses, in solid polymers, and in the form of compact films undergo no visible changes for two years, and glycerol solutions withstand exposure to air at room temperature for 10 days.

The developed method of phototosynthesis is based on the following theoretical propositions [3, 7–9]. Excitation of transition metal complexes in the ligand → metal charge-transfer region causes one-electron reduction of the central ion, which, under certain conditions, results in formation of zero-valent forms and nanoparticles of the metals:

$$[M^{z+}L_n]_s \overset{h\nu}{\rightleftarrows} \{M^{(z-1)+}L_{n-1}, L^{\cdot}\}_s \longrightarrow [M^{(z-1)+}L_{n-1}]_s + L + S^{\cdot}, \quad (1)$$

$$[M^{(z-1)+}L_{n-1}]_s \overset{h\nu,\ S^{\cdot}}{\rightleftarrows} (M^0)_s \overset{}{\rightleftarrows} (M^0_N)_s, \quad (2)$$

1070-3632/02/7204-0642 $27.00 

where M is metal, L ligand, and S solvent. The use of highly light-sensitive complexes and accepting matrices (solvents), which function as "secondary" reductants of intermediates, promotes effective formation of small metal particles.

Preliminary tests with various metal complexes showed that only those complexes could be used as initial ones where the quantum yield of reaction (1) was not lower than 0.1. This requirement is satisfied by complexes containing "good" electron donors in the inner or outer sphere, such as anions of carboxylic and aminocarboxylic acids, as well as tetraphenylborate ion, in particular, copper(II) tetraphenylborate bisethylenediamine $[Cuen_2](BPh_4)_2$. Along with $[Cuen_2](BPh_4)_2$, the following compounds were chosen for preparing photolytes: $[Cuen_2]SO_4$, $AgNO_3$, $[Ag(NH_3)_2]BF_4$, $[Agen_2]BF_4$, $HAuCl_4$, $[Auen_2]Cl_3$, $[Nien_3](BPh_4)_2$, $[Pden_2](BPh_4)_2$, and $Pd(ClO_4)_2$.

It was established experimentally that the character of the process and the composition of the resulting colloids depend on the photolyte composition, the concentration of the light-sensitive metal complex, the energy and intensity of light, the geometry of the reaction vessel, and the presence of oxygen in the system.

To obtain optically transparent homogeneous films of colloidal metals, we used photolyte layers with a thickness of no more than 1–2 mm, monochromatic ($\lambda_{exc}$ 254 nm) and unfiltered light with an intensity of no less than $5 \times 10^{15}$ quantum $cm^{-2}$ $s^{-2}$.

In parallel with the process of photodeposition of films on the surface of a solid carrier, metallic colloids are also formed in bulk photolyte. To obtain dispersions in bulk photolyte, decreased light intensity, decreased concentration of initial metal complex, increased photolyte layer thickness, and/or increased photolyte viscosity (addition of glycerol or ethylene glycol) were used, with simultaneous deaeration (barbotage of argon, helium, and nitrogen). Viscous matrices are preferred, since they hinder colloid aggregation and oxidation. For example, colloidal dispersions of copper are stable no longer than for 10–15 min when obtained in 2-propanol and *N*,*N*-dimethylformamide (DMF) and up to 48 h when obtained in DMF : glycerol = 1 : 10.

Operative control of photosynthesis was performed by spectrophotometry. This method is rather informative here, since colloidal metal particles 1–100 nm in size exhibit specific plasmon absorption in the visible range. The position of the maximum and the intensity and shape of the plasmon bands are suitable qualitative criteria for the structure of colloidal particles and nanophase materials.

From the dependences of the optical density of colloidal films on the surface coverage *q* (obtained from microphotographs and microprobe analysis data) and on the assumption that nanoparticles are spherical, i.e. film thickness is determined by the diameter of particles constituting the film, estimated the extinction coefficients of colloidal metals, $l\ mol^{-1}\ cm^{-1}$: 5200 (gold), 5800 (silver), 6400 (copper), 4800 (nickel), and 4600 (palladium). These values were used for calculating the quantum yields of formation of metallic colloids.

**Gold.** Irradiation of a thin layer (~1 mm) of a solution of HAuCl4 in DMF through a quartz glass contacting the solution, leads to photoinduced growth of a thin optically transparent film on the quartz surface.

Characteristic changes in the UV spectrum of the photolyte and of gold films are shown in Fig. 1. As seen, on first stages, irradiation of the $HAuCl_4$ solution leads to attenuation of the strong absorption at $\lambda_{max}$ 325 nm (Fig. 1, curves *1* and *2*), corresponding to photoreduction of Au(III) to Au(I). Gold nanoparticles begin to form in solution (curve *3*) and, after a short period of time, on quartz surface (Fig. 1, curve *4*), which is detected by the appearance of a monotonic structureless band related, according to [10], to metastable gold clusters 1–1.5 nm in size. Further cluster growth, with formation of colloidal gold, shows up in the appearance and growth of a plasmon peak at 560 nm. The colloid concentration in bulk photolyte attains a maximum after 30-min exposure (Fig. 1, curve *5*) and then decreases due to particle sedimentation. The absorbance of the colloid film on quartz surface monotonically increases, attaining ~2.0 D after 45 min. The fact that the positions of the plasmon peak for the colloid phase in photolyte bulk and on quartz surface are identical gives evidence for close sizes of both colloid particles. However, electron microscopy indicate higher monodispersity of the adsorbed colloid as compared with the bulk one. Interestingly, the degree of film monodispersity increases with irradiation time. This is confirmed by the curves of particle size distribution in films (Fig. 2), obtained on irradiation for 20 and 30 min. As seen from Fig. 2, increasing photolysis time increases a 15–20-nm fraction of particles which are the most stable under the given conditions.

The film-formation process begins with formation of isolated colloidal particles on certain parts of quartz surface. Then, free quartz areas are coated due to formation of new particles and their agglomeration. For gold, the optical density in the plasmon peak region (1.2 D) corresponds to a 100% surface coverage. Using more intense luminous fluxes yields films with

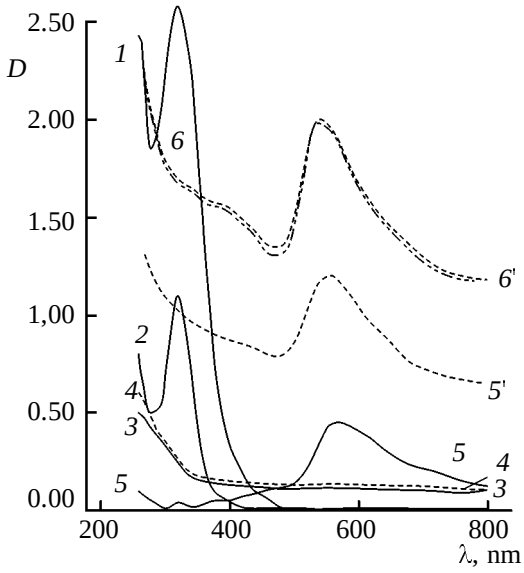


**Fig. 1.** Variation in the absorption spectrum of the photolyte (solid line) and of the gold film deposited on quartz surface (dotted line) on photolysis of a 0.01 M solution of $HAuCl_4$ in DMF at $\lambda_{exc}$ 254 nm ($I$ $4.2\times10^{16}$ quantum $cm^{-2}$ $s^{-1}$, photolyte layer thickness 1 mm). Irradiation time, min: photolyte: (*1*) 0, (*2*) 5, (*3*) 10, (*4*) 12, (*5*) 30, and (*6*) 45; films: (*5*') 30 and (*6*') 45.

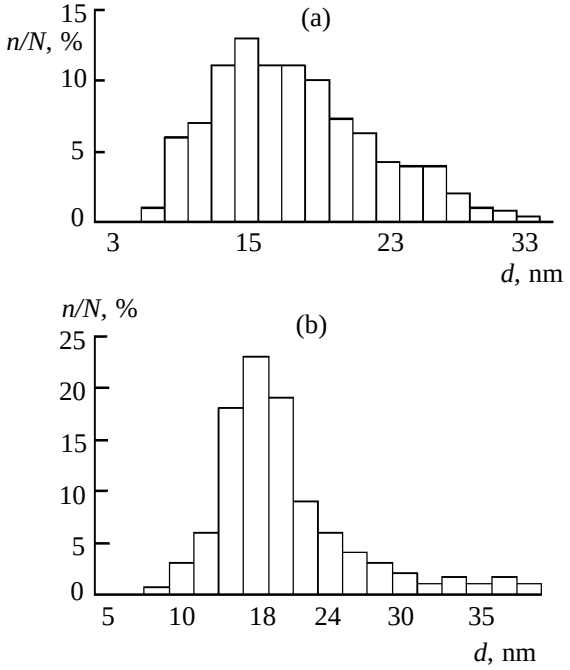


**Fig. 2.** Curves of size distribution of gold particles in the films obtained on photolysis of a 0.01 M solution of $HAuCl_4$ in DMF for (a) 20 and (b) 30 min ($\lambda_{exc}$ 254 nm, $I$ $4.2\times10^{16}$ quantum $cm^{-2}$ $s^{-1}$, photolyte layer thickness 1 mm).

an optical density of up to 3–4 D, i.e. three-dimensional structures caused by deposition of several particle monolayers. Importantly, the films maintain nanophase structure, high uniformity, and transparency throughout the process.

Diffraction measurements showed that, in parallel with increasing number of particles in the film, their structure also changes. Amorphous particles that prevail on the initial stage then transform into crystal line ones. The crystallization process develops during 24 h and do not influence the optical properties of the films (Fig. 1, curve *6*'). The calculated lattice constants for gold submicrocrystals are identical to those for corresponding bulk metals.

As shown by X-ray photoelectron spectroscopy, the films of colloidal gold on quartz, obtained from DMF solutions of $AuCl_4^-$, contain chlorine and nitrogen admixtures (Fig. 3). This can be related to the $AuCl_4^-$ anions adsorbed on the surface of nanoparticles (the presence of a characteristic Au(III) peak at 93.7 eV and DMF) or to their oxidation products. At the same time, these and other admixtures were not detected by microprobe analysis. As follows from the X-ray photoelectron spectra, the bonding energy of 4*f* electrons in the colloidal particles (90.2 eV) is considerably higher than in a crystal of bulk gold (84.0 eV).

Gold films are formed not only via photoinduced growth of nuclei on quartz, but also via dark adsorption from the near-surface layer of clusters 1.0–1.5 nm in size. This follows from the experimental data presented in Fig. 4. A dispersion of gold clusters, obtained by photoreduction of $HAuCl_4$ in DMF and characterized by diffuse broad absorption in the range 560–800 nm (Fig. 4a, curve *1*), was placed in a clean quartz cell and kept in the dark. After 2 h, the bulk sol practically completely transformed into an optically transparent film on cell walls, that exhibited well-defined plasmon absorption (Fig. 4, curve *3*); $\lambda_{max}$ 610 nm). By contrast, the formed colloidal gold particles are not prone to adsorption, i.e. do not yield films (Fig. 4b). In this case, the bulk colloid decomposes via aggregation and subsequent particle sedimentation to form a loose black precipitate at the cell bottom. Thus, sorption of small gold particles from bulk photolyte contributes to formation of colloidal films of gold on quartz.

At equal light intensity and other conditions, the effectiveness of deposition of gold films on quartz is 4 times higher under irradiation at $\lambda_{exc}$ 254 nm than

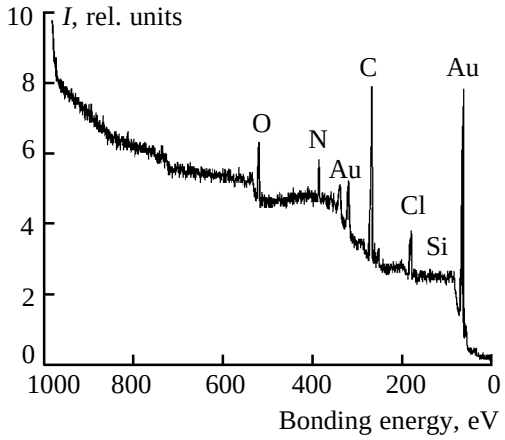


**Fig. 3.** X-ray photoelectron spectrum of the film of colloidal gold photodeposited on quartz (*q* 80%).

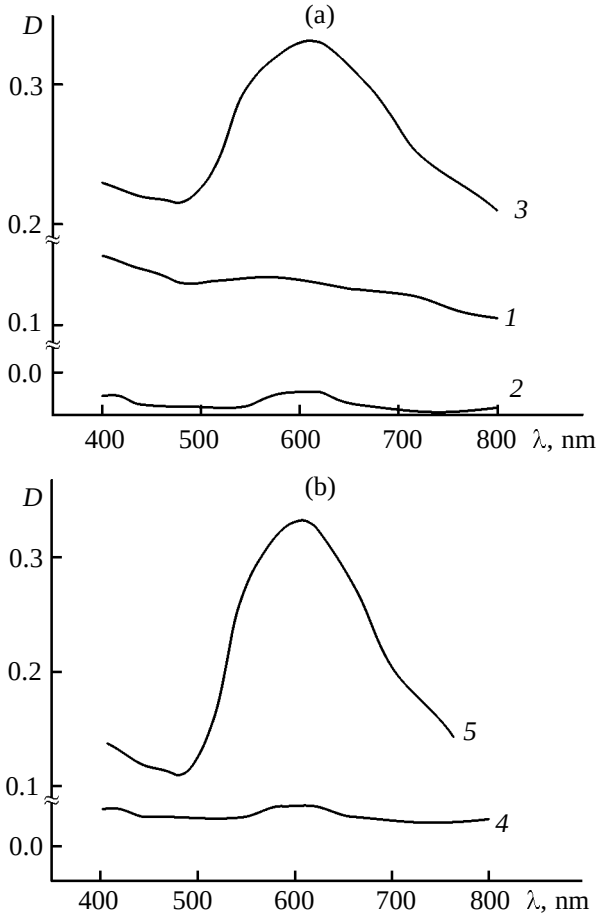


**Fig. 4.** (*1*) Freshly prepared dispersions irradiated for 10 min and (*2*) kept in the dark for 2 h; and (b): (*4*) freshly prepared dispersions irradiated for 20 min and (*5*) kept in the dark for 2 h. (*3*) Spectrum of colloidal gold adsorbed on quartz surface.

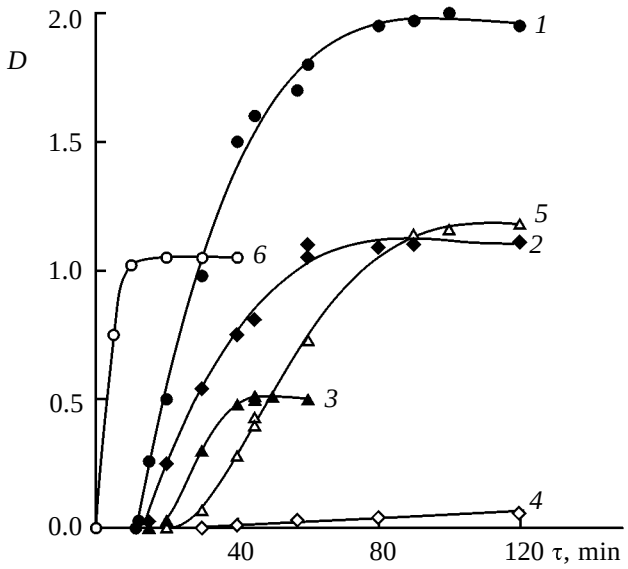


**Fig. 5.** Kinetic curves of photochemical formation of colloidal gold films on quartz from 0.01 M DMF solutions of (*1*–*5*) $HAuCl_4$ and (*6*) $[Auen_2]Cl_3F$ (*l* 1 mm). Exciting light intensity, quantum $cm^{-2}\ s^{-1}$: (*1*, *6*) $4.2\times10^{16}$, (*2*) $1.2\times10^{16}$, (*3*) $7.0\times10^{15}$, (*4*) $8.0\times10^{14}$ ($\lambda_{exc}$ = 254 nm), and (*5*) $3.0\times10^{16}$ (unfiltered light).

under irradiation with unfiltered light. In the latter case, the induction period is almost 1.5–2 times longer (Fig. 5) and the average particle size increases until compact metallic films of bulk gold are formed. This shows up in appearance of a characteristic absorption band in the spectrum (Fig. 6a, curve *5*). Nevertheless, such colloidal films are characterized by a high degree of monodispersity (Table 1) on the initial stage of photolysis (up to 90 min.). Excitation of the solution at $\lambda_{exc}$ 365 nm is ineffective and yields no film. In this case, the process terminates on the stage of formation of Au(I) complexes for which the light with $\lambda_{exc}$ 365 nm is not actinic.

Deposition of gold particles on quartz occurs only if the light intensity exceeds $\sim1.0\times10^{15}$ quantum $cm^{-2}\ s^{-1}$ (Fig. 5). The existence of an intensity threshold is explained by the fact that the photochemical reduction of Au(III) and Au(I) to Au(0) is accompanied by dark reoxidation of the resulting atoms and small nuclei. As a consequence, increasing intensity results in regular increase in the quantum yields of formation of a nanophase gold film on quartz (Table 1). In addition, increasing intensity favors decreased average particle size and improved uniformity of the nanophase covering. For example, at light intensities higher than $4.2\times10^{16}$ quantum $cm^{-2}\ s^{-1}$ one can obtain gaily colored uniform coverings of colloidal gold on quartz with

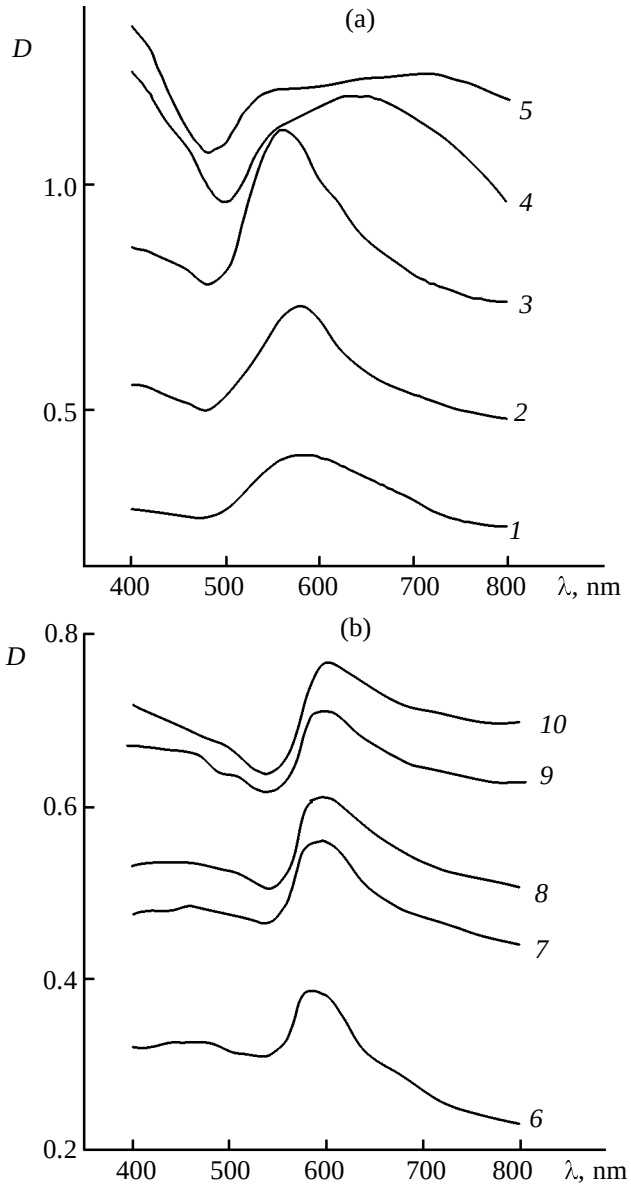


**Fig. 6.** Absorption spectra of nanophase films of (a) gold and (b) copper on quartz obtained on irradiation with unfiltered light ($I = 3.0 \times 10^{16}$ quantum $cm^{-2}$ $s^{-1}$, $l$ = 1 mm) of a 0.01 M solution of $HAuCl_4$ in DMF and of a 0.05 M solution of $[Cuen_2](BPh_4)_2$ in DMF. Surface coverage, % (irradiation time, min): (a): (*1*) 45 (30), (*2*) 60 (45), (*3*) 95 (90), (*4*) >100 (120), and (*5*) >100 (180); and (b): (*6*) 24, (*7*) 37, (*8*) 40, (*9*) 47, and (*10*) 52.

$D_{max} > 2$, which corresponds to the coverage degree ~100% and implies formation of three-dimensional structures. The hypsochromic shift of the plasmon bands from 620 to 540 nm corresponds to the decrease in the particle size from 30–40 to 10–20 nm with increasing light flux intensity. The quantum yields of formation of gold films regularly increase with increasing concentration of the initial gold complex (Table 1).

As the concentration of the initial Au(III) complex in the photolyte is increased within the range $(2.5–5) \times 10^{-3}$ M, the plasmon absorption maximum shifts bathochromically from 520 to 600–620 nm, which suggests increased average (photostable) particle size. Raising of the initial complex concentration above $5 \times 10^{-3}$ M produces the inverse effect: the average particle size decreases and shows up in the hypsochromic shift of plasmon film absorption from 600–620 to 560 nm.

With $[Auen_2]Cl_3$ as initial complex, the induction period of film formation becomes shorter (Fig. 5) and colloid formation mostly occurs in photolyte bulk. To all appearances, here ethylenediamine plays the role of a secondary reducing agent, favoring fast formation of nuclei and their further growth to colloidal particles. Herewith, cluster growth and sedimentation of colloidal particles in photolyte bulk precede cluster diffusion to quartz surface.

The effectiveness of film formation of quartz surface is much unfavored (effective quantum yield $\Phi_{col} < 10^{-3}$) by addition to DMF solutions of stronger (compared with DMF) secondary reducing agents, such as 2-propanol and acetone ($10^{-4}$ M), and also by replacement of DMF by acetone, 2-propanol, methanol, or ethanol. In this case, fast formation and growth of nuclei of the colloidal phase in the bulk is observed. The latter process is faster than particle adsorption on quartz surface. Herewith, dispersions tending for aggregation are formed, sedimenting to give loose precipitates. The particle size in colloidal films varies over a wide range. The average particle size in such films ($\lambda_{max}$ 580–600 nm) is larger than in films obtained in DMF.

As seen from Table 1, the increase of the photolyte layer thickness $l$ from 0.2 to 10 mm does not influence the average size of film-forming particles. The dependence of $\Phi_{col}(n)$ on layer thickness has an extremum. The induction period of colloidal gold formation monotonically increases with $l$, attaining 8 min at $l$ 0.2 mm, 12 min at $l$ 1.0 mm, and 45 min at $l$ 10 mm.

**Silver**. Solutions of $AgNO_3$, $[Agen]BF_4$, and $[Ag(NH_3)_2]BF_4$ in DMF ($\lambda_{exc}$ 254 nm) were used for preparing insular silver films. Preliminary deaeration was not applied. As seen from Fig. 7a, the onset of formation of a film of colloidal silver ($\lambda_{max}$ 440 nm) on quartz contacting a photolyte is associated with appearance of a low-intensity band ($\lambda_{max}$ 345 nm). According to [11], this absorption relates to silver clusters about 1 nm in diameter. Interestingly, these

**Table 1.** Average particle sizes ($d$) and effective quantum yields ($\Phi_{col}$) of gold film deposition from DMF solutions at varied photolysis conditions ($\lambda_{exc}$ 254 nm and unfiltered light)

| Initial complex | $C_{comp}$, M | Layer thickness $l$, mm | $I_l$, quantum $cm^{-2}$ $s^{-1}$ | $d$, nm | $\Phi_{col}$ |
|---|---|---|---|---|---|
| $HAuCl_4$ | $2.5\times10^{-3}$ | 1.0 | $4.2\times10^{16}$ | 10–15 | $2\times10^{-2}$ |
| $HAuCl_4$ | $5\times10^{-3}$ | 1.0 | $4.2\times10^{16}$ | 30–40 | $4\times10^{-2}$ |
| $HAuCl_4$ | $1\times10^{-2}$ | 1.0 | $4.2\times10^{16}$ | 10–20 | $1\times10^{-1}$ |
| $HAuCl_4$ | $1\times10^{-2}$ | 1.0 | $1.2\times10^{16}$ | 20–30 | $8\times10^{-2}$ |
| $HAuCl_4$ | $1\times10^{-2}$ | 1.0 | $7.0\times10^{15}$ | 30–40 | $5\times10^{-2}$ |
| $HAuCl_4$ | $1\times10^{-2}$ | 0.2 | $4.2\times10^{16}$ | 10–20 | $4\times10^{-3}$ |
| $HAuCl_4$ | $1\times10^{-2}$ | 10.0 | $4.2\times10^{16}$ | 10–20 | $6\times10^{-3}$ |
| $[Auen_2]Cl_3$ | $1\times10^{-2}$ | 1.0 | $4.2\times10^{16}$ | 30–50 | $2.6\times10^{-1}$ |
| $HAuCl_4$ | $1\times10^{-2}$ | 1.0 | Unfiltered light, $3.0\times10^{16}$ | 30–50 | $5\times10^{-2}$ |

highly reactive intermediates are rather stable in the adsorbed state and withstand exposure of the support to air for 10–15 min. Growth of adsorbed clusters and coverage of the surface with silver nanoparticles is accompanied by improving film structure at maintaining the average particles size ($\lambda_{max}$ const). As with gold, increased photolyte viscosity causes colloidal silver formation mainly in the bulk of the liquid phase. In 1:1 glycerol:DMF mixtures, the same silver clusters ($\lambda_{max}$ 345 nm) are formed, stable in the dark up to 35 min. In more viscous systems at a 9:1 glycerol:DMF ratio, clusters with $\lambda_{max}$ 325 nm (Fig. 7b, curves *1* and *2*) are formed, which, according to [12], have the composition $Ag_9^+$. The shift of the maximum from ~440 to 460 nm and the shape of the plasmon bands indicate that bulk silver dispersions are less uniform compared with solid films and contain both low-atomic clusters and large colloidal agglomerates (long-wave branch of the band). The use of rigid matrices, solid polymeric layers of polyvinyl alcohol, polyethylene glycol, and gelatin, prolongs the lifetime of intermediates. For example, the $Ag_9^+$ and $Ag_n$ clusters ~1 nm in diameter, photogenerated in polyvinyl alcohol, are stable on exposure of irradiated samples to air in the dark for more than two days.

In contrast to the above gold clusters and small particles, silver clusters give characteristic absorption bands in the UV range. This is caused by the electronic structure of the metal, namely, by the fact that its dielectric permittivity is contributed by free electrons only, whereas in copper and gold bound electrons are also involved.

From electron microscopy data and the shape of the plasmon bands of photoinduced silver colloids (Fig. 8) it follows that the internal structure of the latter depends on the nature of the initial complex. Under the same conditions, replacement of $AgNO_3$ by $[Ag(NH_3)_2]BF_4$ results in decreased average particle size and increased degree of monodispersity of the nanophase system. With $[Agen]BF_4$ (Fig. 8, curve *2*), chain agglomerates characterized by two-band absorption are formed [10]. This could be explained by the ability of the bidentate ligand to form polynuclear complexes, precursors of metal clusters, on one side, and by the higher reductive power of ethylenediamine, as compared with ammonia, in finishing reduction of intermediates, on the other. Indeed, in contrast with stable $[Ag(NH_3)_2]^+$, the complex $[Agen_2]^+$ tends to dark reduction in alcoholic matrices (2-propanol, glycerin, polyvinyl alcohol). For example, in the solid polyvinyl alcohol, small amounts of $Ag_9^+$ and $Ag_n$, ~1 nm in diameter, are found already on in the process of drying photolayers for 30 min. At the same time, as seen from Table 2, in the case of silver, replacing ammonia by ethylenediamine in the inner sphere only slightly influences the quantum yields of formation of silver films.

By contrast, the quantum yield of colloidal silver more than doubles when passing from $[Ag(NH_3)_2]^+$ to $[Ag(DMF)_2]^+$ (solution of $AgNO_3$ in DMF). As in the case of gold, both $\Phi_{col}$ and the degree of monodispersity of film particles increase with light intensity, and freshly prepared silver nanoparticles undergo transformation from the amorphous state to crystalline. The lattice constants calculated for silver submicrocrystals are identical to those for bulk metal.

According to the data of X-ray photoelectron spectrosocopy, the bonding energy of 3*d* electrons is considerably higher for silver colloids (373.0 eV) than for bulk crystals (368.1 eV) and depends on particle

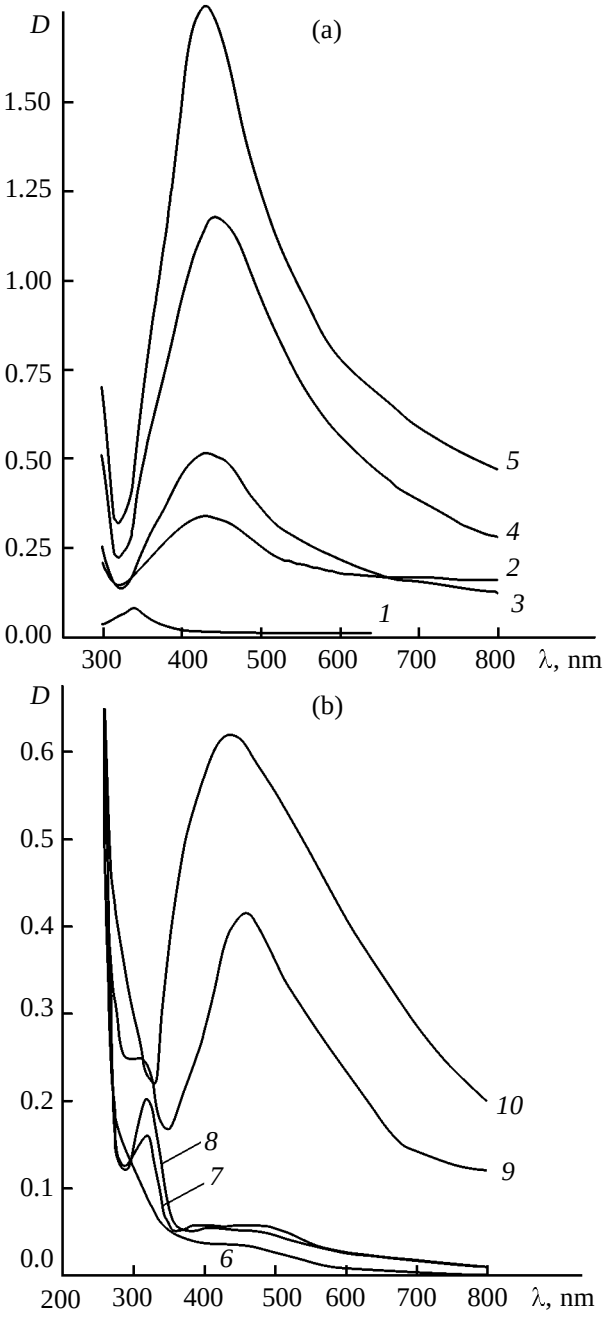


**Fig. 7.** Variation of the absorption spectrum of silver nanoparticles on photolysis of (a) a solution of $[Ag(NH_3)_2]BF_4$ (*C* 0.01 M) in DMF and (b) a solution of $AgNO_3$ (*C* 0.01 M) in glycerol : DMF, 9 : 1. $\lambda_{exc}$ 254 nm, *I* $4.2 \times 10^{16}$ quantum $cm^{-2}$ $s^{-1}$, *l* 1 mm. (a) Adsorbed films, and (b) bulk dispersions. Irradiation time, min: (*1*) 2, (*2*) 5, (*3*) 10, (*4*) 20, (*5*) 45; (*6*) 0, (*7*) 0.5, (*8*) 1.5, (*9*) 5, and (*10*) 25.

size. As the particle size increases, the bonding energy approaches its value for bulk samples. The X-ray photoelectron spectra also showed the presence of 5–7% of $Ag_2O$ in the silver films (maximum at 535.3 eV).

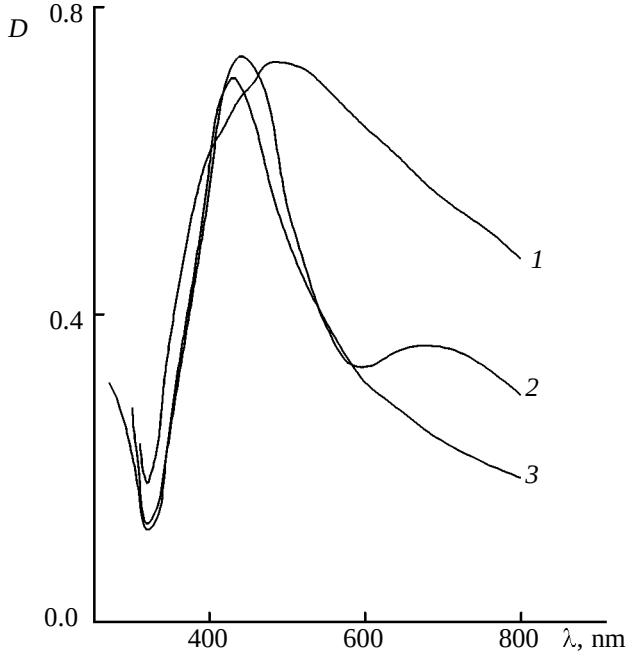


**Fig. 8.** Absorption spectra of silver nanophase films obtained from 0.01 M solutions of (*1*) $AgNO_3$, (*2*) $[Agen]BF_4$, and (*3*) $[Ag(NH_3)_2]BF_4$ in DMF ($\lambda_{exc}$ 254 nm, *l* 1 mm, *I* $4.2 \times 10^{16}$ quantum $cm^{-2}$ $s^{-1}$).

**Copper**. The formation of films of colloidal copper on quartz surface has a number of peculiarities. Firstly, film growth is accompanied by increase in the size of film-forming particles, which is seen from a bathochromic shift of plasmon absorption. Under certain conditions, this shift can attain 100 nm and more. Secondly, in contrast with gold, nanoparticle formation occurs in the presence of the initial Cu(II) complex in the photolyte. Figure 9 shows characteristic changes of the absorption spectrum of films of colloidal copper, formed under UV irradition on a quartz plate in contact with a DMF solution of $[Cuen_2] \cdot (BPh_4)_2$. Film formation begins with adsorption of nuclei that, as in the case of gold, have no characteristic absorption bands in the near UV and visible spectral range, on account of their specific electronic structure [10]. Cluster growth and appearance of single particles on quartz surface give rise to a weak plasmon peak at 610 nm. On this stage, the insular film (surface coverage ~17 %) is characterized by a wide particle size distribution with a maximum near 30 nm, as is seen from Fig. 10. Then the average particle size slightly increases up to ~40 nm and no longer changes up to 80–100% surface coverage, i.e. up to formation of a colloidal monolayer. Interestingly, the degree of film monodispersity increases on this stage. Further film growth, i.e. deposition of nano-

particles on already existing particles, shifts the plasmon peak to 680–720 nm and renders it broader. According to theory, this is related to an essential contribution of interparticle interaction which is in any case stronger than on formation of compact three-dimensional structures of gold and silver nanoparticles. The particle agglomeration that shows up in broadening and bathochromic shift of the plasmon peak is the weaker the higher light intensity. For example, the copper films ($D_{max}$ ~2) obtained from a 0.05 M solution of $[Cuen_2](BPh_4)_2$ in DMF under irradiation at $I$ $4.2 \times 10^{16}$ quantum $cm^{-2}$ $s^{-1}$ give a well-defined peak at 650 nm. This means that the film comprising about two monolayers preserves the nanophase structure.

The absence of plasmon absorption in the spectrum of irradiated photolyte after photolysis indicates that colloidal copper is deposited only on the solid surface and does not form in photolyte bulk, as it was observed with silver and gold. Probably, this is caused by the high activity of small copper clusters that are rapidly oxidized in photolyte bulk by solute oxygen and photolysis products. At the same time, the surface acts as a stabilizer of growing particles.

The effectiveness of deposition of copper films on quartz is 1.5–2 times higher under irradiation with light with $\lambda_{exc}$ 254 nm than under irradiation with unfiltered UV light of approximately the same intensity. Unfiltered light causes formation of films of metallic copper ($\Phi_{col}$ 0.03) with a characteristic spectrum represented in Fig. 6b. Under excitation with $\lambda_{exc}$ 365 nm the initial Cu(II) complex but, as with silver and gold, no colloidal metal is formed. In this case, the process finishes on the stage of formation of Cu(I) compounds.

Low-energy electron diffraction showed that the films contain a crystalline form. The lattice constants calculated for copper submicrocrystals are identical to those for bulk metal.

In the systems studied, collidal copper is formed only at high light intensities. As seen from Table 3, the minimum threshold light intensity is ~$8.0 \times 10^{14}$ quantum $cm^{-2}$ $s^{-1}$ at $\lambda_{exc}$ 254 nm. Within the intensity range $(3.0–7.0) \times 10^{15}$ quantum $cm^{-2}$ $s^{-1}$, the reaction quantum yield is considerably lower than the quantum yield of Cu(I) on photolysis of $[Cuen_2] \cdot (BPh_4)_2$ in alcohols and DMF ($\Phi_{Cu(I)}$ = 0.8). Thus, the secondary reactions of conversion of Cu(I) to Cu(0) and, further, to stable colloidal particles essentially limit the process rate. At light intensities higher than ~$4.2 \times 10^{16}$ quantum $cm^{-2}$ $s^{-1}$, photodegradation of colloidal copper particles concurs with their formation, which adversely affects the quantum yield of the main reaction (Tables 3 and 4). The influence of

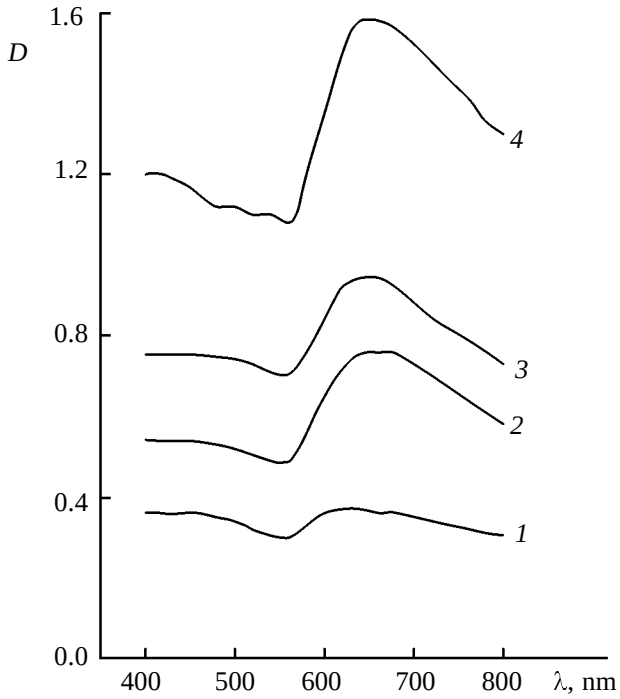


**Fig. 9.** Absorption spectra of nanophase copper films at various coverages of quartz surface, obtained from a 0.05 M solution of $[Cuen_2](BPh_4)_2$ in DMF ($\lambda_{exc}$ 254 nm, $I$ $1.5 \times 10^{16}$ quantum $cm^{-2}$ $s^{-1}$, $l$ 0.2 mm). Quartz surface coverage, %: (*1*) 17, (*2*) 50, (*3*) 64, and (*4*) 100.

**Table 2.** Effective quantum yields ($\Phi_{col}$) of formation of silver films deposited from a 0.01 M solution in DMF at various photolysis conditions ($\lambda_{exc}$ 254 nm, $l$ 1 mm) and initial complexes

| Initial complex | $I_l$, quantum $cm^{-2}$ $s^{-1}$ | $\Phi_{col}$ |
|---|---|---|
| $AgNO_3$ | $4.2 \times 10^{16}$ | 0.38 |
| $[Ag(NH_3)_2]BF_4$ | $4.2 \times 10^{16}$ | 0.17 |
| $[Ag(NH_3)_2]BF_4$ | $1.2 \times 10^{16}$ | 0.1 |
| $[Ag(NH_3)_2]BF_4$ | $0.7 \times 10^{15}$ | 0.04 |
| $[Agen_2]BF_4$ | $4.2 \times 10^{16}$ | 0.21 |

light intensity on degree of monodispersity obeys a regularity common for the three metals: increasing intensity leads to increasing degree of monodispersity of colloidal copper films (Table 4).

It is seen from Fig. 11 and Table 3 that the concentration of the initial Cu(II) complex essentially influences the rate of formation and the properties of copper colloids. Within the range 0.01–0.25 M, the

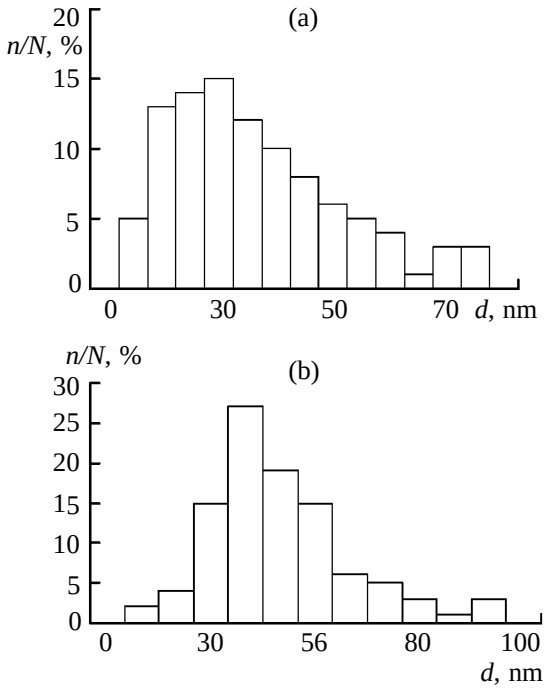


**Fig. 10.** Size distribution curves for copper particles in the films obtained on photolysis of a 0.05 M solution of $[Cuen_2](BPh_4)_2$ in DMF ($\lambda_{exc}$ 254 nm, $I$ $1.5\times10^{16}$ quantum $cm^{-2}$ $s^{-1}$, $l$ 0.2 mm). Quartz surface coverage, %: (a) 17 and (b) 65.

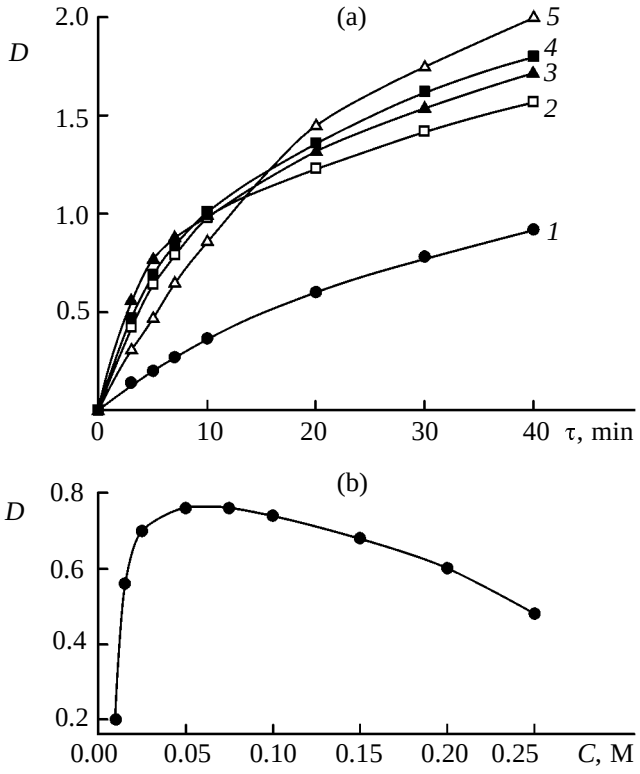


**Fig. 11.** (a) Kinetic curves and (b) relative rates of deposition of colloidal copper on quartz at various concentrations of $[Cuen_2](BPh_4)_2$ in the photolyte. Concentration, M: (*1*) 0.01, (*2*) 0.025, (*3*) 0.075, (*4*) 0.1, and (*5*) 0.25. $I$ $7.0\times10^{15}$ quantum $cm^{-2}$ $s^{-1}$, $\lambda_{exc}$ 254 nm, $l$ 0.2 mm.

concentration dependence of the relative particle size (the criterion of plasmon $\lambda_{max}$) is extremal. As was already shown, there are similar regularities for gold colloids.

Small glycerol additives (DMF : glycerol 30 : 1 by volume) leads to increased quantum yields of formation of colloidal copper films, which is probably caused by a higher stability of intermediate clusters. Further increase of the glycerol content and, correspondingly, of the viscosity of the photolyte decreases the effectiveness of film formation, which can be explained, as in the case of gold, by diffusion restrictions. 2-Propanol additives favor particles formation in photolyte bulk.

Investigation of the effect of initial complex nature showed that film formation from DMF solutions of $[Cuen_2]SO_4$ is 20 times slower than from DMF solutions of $[Cuen_2](BPh_4)_2$, other conditions (concentration, light intensity, $\lambda_{exc}$) being equal. As judged from the plasmon $\lambda_{max}$, the average particle size is lower in the case of $[Cuen_2]SO_4$, but the resulting film is characterized by a wide particle size distribution.

**Nickel**. Investigation of the photochemical synthesis of nickel colloids from DMF solutions of $[Nien_3](BPh_4)_2$ showed that here film deposition on quartz begins after a prolonged induction period, which is caused by the high stability of the complex. For example, the incubation period is 40 min at solution concentrations of 0.05 M. The optical density of the films attains 0.5 D.

According to the data of electron microscopy, film formation begins with formation of isolated colloidal particles on some areas of the surface. The average particle size is 30–40 nm. Further irradiation causes particle growth up to ~50 nm and particle assembling into rings. The particle size no longer increases in course of photolysis, implying that the 50-nm size is photostable for nickel colloids. Around ring apertures, ring growth steps of hexagonal shape, as well as formed crystals. The torus size is 110–160 nm, and the aperture size is 20–40 nm. Further coverage of

**Table 3.** Effective quantum yields ($\Phi_{col}$) of formation of colloidal copper films under various conditions ($\lambda_{exc}$ 254 nm, $l$ 1 mm)

| $C_{comp}$, M | Solvent | $I_l$, quantum $cm^{-2}$ $s^{-1}$ | | | | |
|---|---|---|---|---|---|---|
| | | $8.0 \times 10^{14}$ | $3.0 \times 10^{15}$ | $6.0 \times 10^{15}$ | $7.0 \times 10^{15}$ | $4.2 \times 10^{15}$ |
| 0.01 | DMF | $<10^{-3}$ | $<10^{-3}$ | $<10^{-3}$ | 0.10 | 0.10 |
| 0.025 | DMF | $<10^{-3}$ | $<10^{-3}$ | 0.14 | 0.31 | 0.26 |
| 0.05 | DMF | $<10^{-3}$ | 0.04 | 0.22 | 0.53 | 0.24 |
| 0.075 | DMF | $<10^{-3}$ | 0.02 | 0.16 | 0.38 | 0.10 |
| 0.10 | DMF | $<10^{-3}$ | 0.02 | 0.13 | 0.36 | 0.08 |
| 0.15 | DMF | $<10^{-3}$ | $<10^{-3}$ | 0.10 | 0.30 | 0.08 |
| 0.25 | DMF | $<10^{-3}$ | $<10^{-3}$ | $<10^{-3}$ | 0.26 | 0.05 |
| 0.05 | DMF–glycerol, 30 : 1 | $<10^{-3}$ | 0.44 | 0.56 | 0.38 | 0.07 |
| | 5 : 1 | $<10^{-3}$ | 0.40 | 0.44 | 0.38 | 0.07 |
| | 2 : 1 | $<10^{-3}$ | 0.38 | 0.30 | 0.30 | 0.07 |
| 0.05 | DMF–2-propanol | $<10^{-3}$ | 0.08 | 0.10 | 0.10 | 0.02 |

**Table 4.** Dependence of the average particle size ($\lambda_{max}$) in copper films deposited from 0.05 M solutions in DMF on photolysis conditions ($\lambda_{exc}$ 254 nm)

| Initial complex | Layer thickness, $l$, mm | $I_l$, quantum $cm^{-2}$ $s^{-1}$ | $\lambda_{max}$, nm |
|---|---|---|---|
| $[Cuen_2](BPh_4)_2$ | 1.0 | $4.2 \times 10^{16}$ | 610–720 |
| $[Cuen_2](BPh_4)_2$ | 1.0 | $6.0 \times 10^{15}$ | 620–720 |
| $[Cuen_2](BPh_4)_2$ | 1.0 | $3.0 \times 10^{15}$ | 640–760 |
| $[Cuen_2](BPh_4)_2$ | 0.2 | $4.2 \times 10^{16}$ | 610–680 |
| $[Cuen_2](BPh_4)_2$ | 10.0 | $4.2 \times 10^{16}$ | 600–640 |
| $[Cuen_2]SO_4$ | 1.0 | $4.2 \times 10^{16}$ | 590 |

free areas proceeds via formation of new particles and their aggregation in rings. Importantly, such film structure is maintained during the whole photolysis and even at a practically complete surface coverage.

According to the data of X-ray photoelectron spectroscopy, the resulting films mainly consist of oxo and hydroxo forms of nickel. This is confirmed by the presence in the X-ray photoelectron spectrum of bands of nickel oxide and hydroxide at 853.4 and 855.5 eV, respectively. The concentrations of these forms increase during irradiation. The quantum yield of formation of the colloidal film is 0.2.

**Palladium**. Photochemical deposition of colloidal films of palladium on quartz from DMF solutions of $[Pden_2](BPh_4)_2$, too, begins after an induction period whose duration is 20–30 min, depending on photolysis conditions. The presence of a colloidal metal phase is confirmed by X-ray photoelectron spectroscopy: The X-ray photoelectron spectrum displays bands at 341.8 and 346.63 eV, characteristic of $Pd^0_n$. According to data of electron microscopy, the films consist of spherical particles forming regular chain structures. The average particles size in the film is ~50 nm.

## BULK DISPERSIONS IN SOLID POROUS AND POLYMERIC MATRICES

The photosynthesis of colloids of copper, silver, gold, and palladium [13, 14] in homogeneous rigid polymeric matrices of polyvinyl alcohol and in pores of silica glasses and fluorocarbon organic membranes from $[Cuen_2](BPh_4)_2$, $[Ag(NH_3)_2]BF_4$, $HAuCl_4$, and $Pd(ClO_4)_2$ revealed the following regularities.

The colloids formed possess the highest degree of monodispersity as compared with all considered before. The increased monodispersity and the shape of plasmon bands give evidence for the absence of agglomeration. In the case of silica glasses and fluorocarbon membranes, the size of nanoparticles is restricted by the size of pores and channels.

In solid polymeric matrices, cluster coalescence

processes are probably hindered by the high viscosity of the matrices and the low mobility of the clusters. The growth of nanoparticles under such conditions is provided by photoreduction of the initial complex on their surface. Decreased concentration of the initial complexes in the photolyte should regularly decrease the size of the nanoparticles. This is fully confirmed by the experimental results showing that a $5 \times 10^{-3}$–$1 \times 10^{-1}$ M decrease in the concentration of the complex causes a hypsochromic shift of the plasmon peak. In view of the position of the plasmon peak, one can suppose that by varying the concentrations of photolytes in polyvinyl alcohol on can obtain particles ≥1 nm in size.

A suitable factor of controlling the structure of colloid particles in polymeric matrices is photolyte viscosity whose variation is determined by the time of photolayer drying. For example, as the time of drying of polyvinyl alcohol films from 20 min to 5 h leads, other factors being equal, the average particle size decreases, as evidenced by the shift of plasmon absorption from 560 to 520 nm for gold, from 420 to 380 nm for silver, and from 580 to 560 nm for copper.

The kinetic curves for formation of metallic colloids in polyvinyl alcohol are similar to those for photodeposition of films on quartz. They include an induction period whose duration decreases with increasing light intensity and complex concentration. The quantum yields of the process on the stage of particle growth are approximately double those on quartz surface under similar conditions. This is explained by the fact that polyvinyl alcohol is an effective secondary reducer for initial Cu(II), Ag(I), Au(III), and Pd(II) complexes and for intermediates. Moreover, polyvinyl alcohol prevents oxidation of low-atomic clusters by oxygen. One would expect that in passing from liquid photolytes to solid polymeric matrices the induction period would get longer. However, this proved the case only with silver. Therefore, the processes of diffusion and reduction of initial metal complexes on the surface of colloid phase nuclei only slightly limit the rate of colloid formation.

All the above regularities also hold for photochemical formation of metallic colloids in polyethylene glycol and gelatin. However, the rate of formation of a silver colloid in polyethylene glycol is about ten times lower than in polyvinyl alcohol. In gelatin, the rate of photochemical reduction of $[Cuen_2] \cdot (BPh_4)_2$ and $HAuCl_4$ is approximately equal to the rate of photoreduction in polyvinyl alcohol, but on the stage of effective growth of nanoparticles, the process rate in gelatin is about two times lower than in polyvinyl alcohol. Probably, this is caused by the presence of sulfur in gelatin, since sulfur is a strong catalytic poison in chemical metal deposition processes [12].

Silver, gold, and palladium colloinds in polyvinyl alcohol films preserve their spectral properties for two years in air in the dark. Copper colloids in polyvinyl alcohol are stable for 2–3 months. On longer storage, the samples decolorize and aquire a slight coloration typical of oxidized forms of copper(II).

## MECHANISM OF PHOTOINDUCED FORMATION OF METALLIC COLLOIDS

Formation of metallic colloids is an intricate multistage process. Scheme (3) illustrates this process by the example of photoreduction of gold at the quartz–$AuCl_4^-$ solution interface.

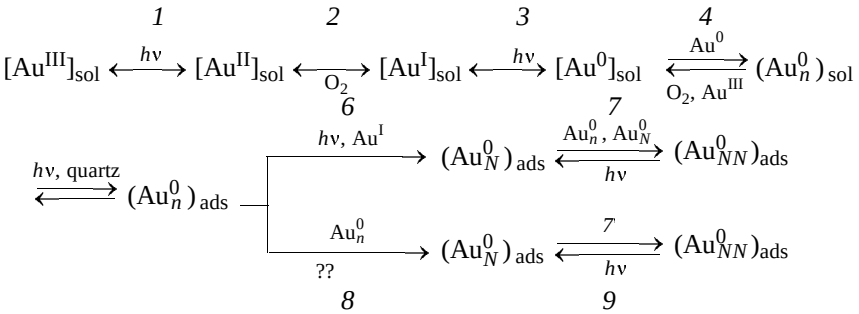


(3)

Here $Au^0_n$ are intermediate clusters ($d \le 1$ nm), $Au^0_N$ are photostable nanoparticles, and $Au^0_{NN}$ are the nanoparticle aggregation products changing the energetic characteristics of the plasmon.

The photoreduction of Au(III) involves initial formation of Au(I) and trace amounts of clusters in the photolyte. In the dark, Au(I) is oxidized by solute oxygen to initial Au(III), which is detected by the

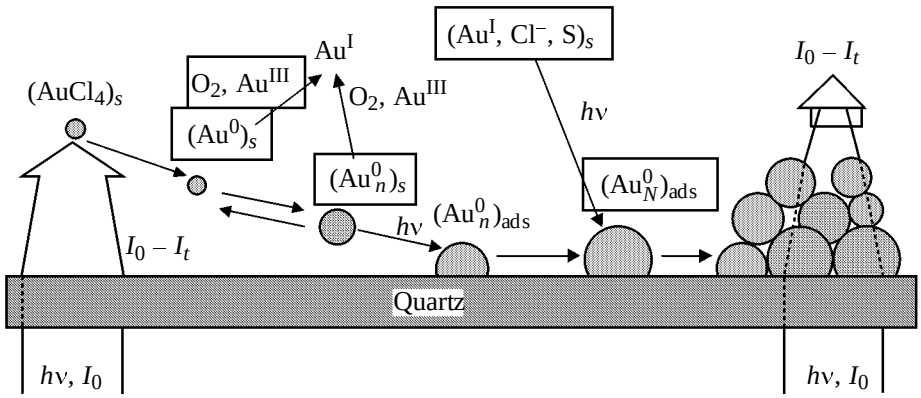


**Fig. 12.** Scheme of photochemical formation of a colloidal metal film on quartz surface.

appearance of characteristic absorption at 325 nm in the spectrum. Irradiation increases the number of metastable clusters $Au_n^0$ first in photolyte bulk and then on the frontal surface of the cell (Fig. 1, curve *12*). Stages *1–5* have an induction period whose duration depends on light intensity (Fig. 5). The existence of a long induction period is largely related to the necessity to reduce all the initial Au(III) complex which, similarly to oxygen, is can effectively oxidize intermediate forms of $Au^0$:

$$2Au^0 + Au^{III}(O_2) \longrightarrow 3Au^I + ... \qquad (4)$$

This is caused by the high reductive potentials $\varphi_0$ of low-atomic metal clusters [15]. For example, the $\varphi_0$ values for the pairs $Ag^+/Ag_1^0$ and $Cu^+/Cu_1^0$ are –1.8 and –2.7 V, i.e. they are much higher than for bulk metals.

The subsequent stages of formation and growth of colloidal particles on quartz surface proceed rather effectively photochemically ($\Phi$ ~0.1) and about 50 times slower in the dark. If the dark process involves adsorption and coalescence of clusters on quartz surface and the coalescence rate is not limited by irradiation, one can assume that the photochemical process has a different mechanism. Indeed, colloidal films of gold formed in the dark are characterized by a larger average particle size. Secondly, the shape of the kinetic curves of photodeposition, corrected for the intrinsic filtering effect (attenuation of exciting light due to formation of a strongly absorbing film on the frontal wall of the cell) points to an autocatalytic nature of the process (Fig. 13). The above results give grounds to state that the intermediate gold clusters and small particles catalyze photoreduction of of Au(I) complexes from photolyte bulk. Catalytic properties of small metallic particles are well known and widely used in chemical (electrodeless) metal deposition from solutions [15]:

$$M^{z+}_{sol} + Red_{sol} \xrightarrow[Cat]{M_l^0} M^0_s + Ox_{sol}. \qquad (5)$$

Depending on the metal, borane, hydrazine, formaldehyde, hypophosphite, glucose, and many other hydrogen-containing compounds can serve as reducers. Such systems (chemical metallization baths) are thermodynamically unstable, and metal deposition in them proceeds until one of the components is exhausted, and the resulting coatings have the structure of bulk metal. A distinguishing feature of the photochemical process under consideration is that the system contains no strong reducer capable of reducing the metal complex in the dark at room temperature. The acceleration of the photochemical reduction of Au(I) in this case can be explained by that the gold clusters and small particles, obtained on the first stages, play the role of typical semiconductors:

$$(Au^0_n)_s \overset{h\nu}{\rightleftarrows} (Au^+_n, e)_s, \qquad (6)$$

$$(Au^+_n, e)_s \xrightarrow{Au^I,\ Cl^-(S)} (Au^0_{n+1}) + Cl^{\cdot}(S^{\cdot}). \qquad (7)$$

The rate of photochemical growth of gold colloids from ethylenediamine gold complexes is higher than for the chloride. This fact can be related to the higher reduction potential of ethylenediamine, as compared with $Cl^-$, in the process of acceptance of the electron–hole pairs formed by photoreduction of gold nanoparticles. The pronounced size dependence of the catalytic properties of metallic nanoparticles explains why the particles grow to a certain (photostable) size in the course of photosynthesis. Further on, increase in the concentration of nanoparticles only occurs in the system, due to appearance and growth of new clusters.

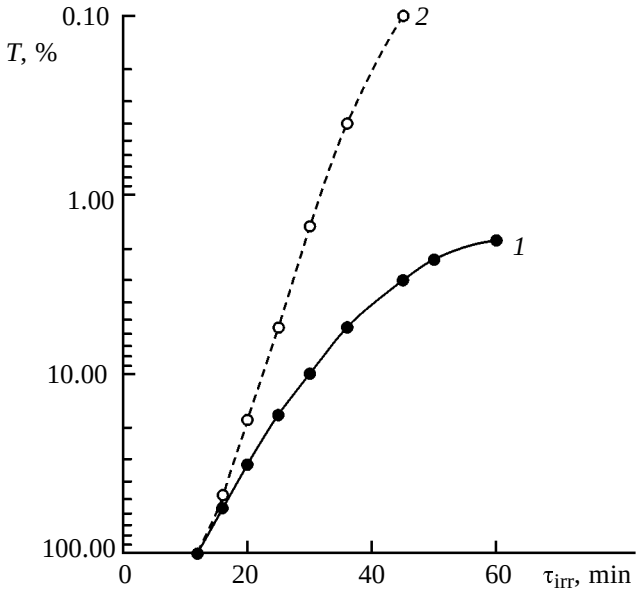


**Fig. 13.** Kinetic curves of formation of colloidal gold on quartz surface. (*1*) Experimental curves and (*2*) the curves corrected for the intrinsic filtering effect.

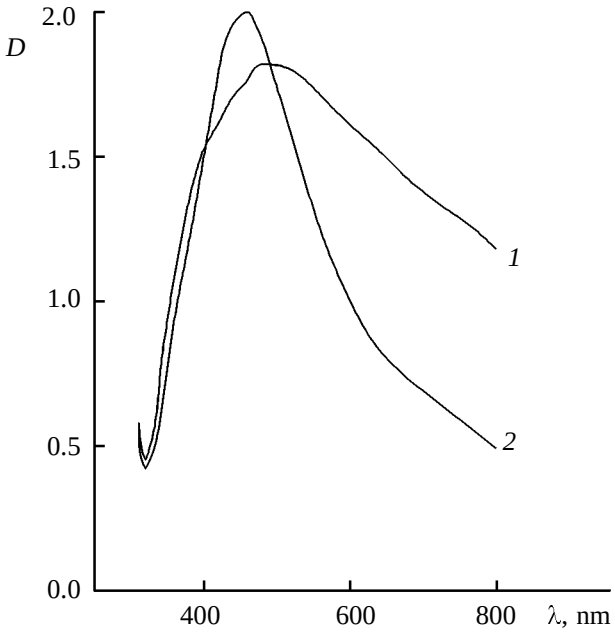


**Fig. 14.** Spectral curves illustrating the effects of light intensity and of photodegradation of "large" particles and agglomerates in photodeposited silver films. (*1*) Freshly prepared film ($I$ $7.0\times10^{15}$ quantum $cm^{-2}$ $s^{-1}$) and (*2*) the same film after irradiation ($\lambda_{exc}$ 254 nm, $I$ $4.2\times10^{16}$ quantum $cm^{-2}$ $s^{-1}$) for 30 min.

The photochemical covering of quartz surface with colloidal gold particles is nicely consistent with the Volmer–Weber mechanism that describes many processes of metal vapor deposition on solid supports. However, there is a distinctive morphological feature of photodeposited continuous gold, silver, and copper films: They preserve their nanophase structure both in the growth process and on further storage. The second peculiarity of photodeposited colloidal metal films is that under intensive light their structure (degree of monodispersity) is improved, which is important for their practical applications, in particular, in lasers. The improvement of the structure of metal colloids is explained by the effect of photodegradation of the loose agglomerates formed by cluster coalescence. Indeed, as seen from Fig. 14, irradiation of freshly prepared silver films with a high-intensity light flux in the absence of photolyte leads to a significant change in the shape of the plasmon bands, in response to increasing degree of monodispersity of the system.

The processes of photosynthesis of colloidal copper and silver, as well as of colloids of these metals in other phase systems, are characterized by similar kinetic regularities. The main difference is that the induction period with copper, silver, and palladium is shorter than with gold (Figs. 5, 11, and 15). This is explained by that the photochemical transition $Ag(I)\rightarrow Ag(0)$ is one-quantum, and, in the case of copper, colloid formation begins in the presence of the initial Cu(II) complex in the photolyte, probably because of the lower redox potential of the pair $[Cu^{II}]/Cu^{0}_{N}$. A peculiar feature of the palladium formation process is that it is highly autocatalytic in nature.

One more feature of photodeposited colloidal films is their strong adhesion to the support. For example, conducting coatings unseparable from the support were obtained on colloidal films on quartz by autocatalytic growth from the chemical copper plating solution containing copper(II) tartrate, formaldehyde, and alkali. The traditional technique employs palladium activators containing hydrolyzed forms of $SnCl_2$. Polynuclear forms of Sn(II) oxo–hydroxo complexes play the role of an intermediate layer that links support surface with metal coating.

The adhesion of copper colloidal films is stronger than of silver, gold, and palladium ones. Probably, this fact probably reflexes the higher polarizability of the Cu(I)–O– bond at the quartz–metal interface and, therefore, the higher affinity to the surface. Thus, the experimental evidence points to specific photoinduced adsorption of growing metal nanoparticles.

## INFLUENCING FACTORS. POSSIBILITIES OF PURPOSIVE PHOTOSYNTHESIS OF COLLOIDS

**Light intensity and energy.** As already shown, all the processes under consideration are characterized

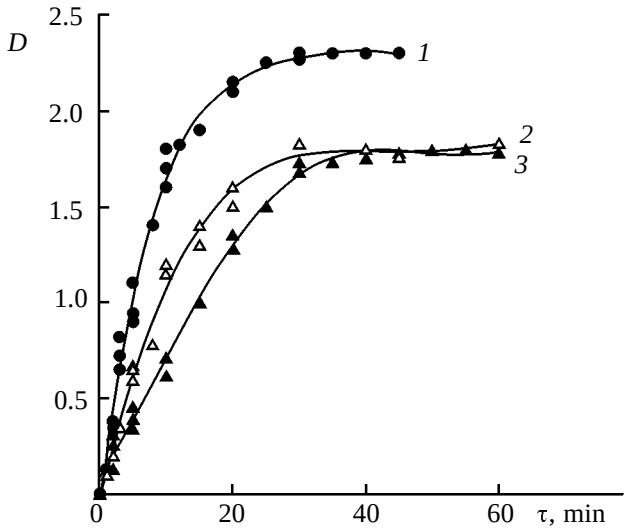


**Fig. 15.** Kinetic curves of deposition of colloidal silver on quartz from 0.01 M DMF solutions of (*1*) $AgNO_3$, (*2*) $[Ag(NH_3)_2]BF_4$, and (*3*) $[Agen]BF_4$ ($I$ $4.2\times10^{16}$ quantum $cm^{-2}$ $s^{-1}$, $\lambda_{exc}$ 254 nm, $l$ 1.0 mm).

by a well-defined threshold intensity of exciting light $I_{th}$ of $\sim10^{15}$ quantum $cm^{-2}$ $s^{-1}$. The steady growth of nanoparticles is possible only when a minimum necessary concentration of nuclei is generated in the photolyte. As a result of the intrinsic filtering effect, strongly absorbing films grow until the light intensity attains $I_0 - I_{abs} \geq I_{th}$. This causes plateaus in the kinetic curves (Figs. 5, 11, and 15). Indeed, the $I_{th}$ values calculated from the plateau heights are identical with those measured experimentally. The plateau height and, correspondingly, the maximum thickness of the resulting film is larger the larger $I_0$. With increasing intensity, the induction period shortens and the effective quantum on the stage of photocatalytic growth of nanoparticles increases. This agrees with the multiphoton mechanism presented in scheme 3. The dependence of $\Phi_{col}$ on $I_0$ is monotonic for gold and silver (Tables 1 and 2). For for copper, there is an extremum at $I$ $7\times10^{15}$ quantum $cm^{-2}$ $s^{-1}$ (Table 3). We explain the latter result by the lower photostability of low-atomic clusters and, as a consequence, by their burning-out at high light intensities.

The above experiments showed that by varying light intensity one can control not only the kinetics of growth of metallic colloids, but also their properties. This is illustrated by the data of Tables 1–4. There is a regularity common for all the metals: The higher light intensity, the smaller average nanoparticle size and the narrower particle size distribution. Better monodispersity is attained by photolysis of large particles and agglomerates by high-intensity light fluxes.

The use of unfiltered UV light worsens monodispersity of copper and gold colloids (Fig. 6), other conditions being equal. It is seen from Fig. 6 that under prolonged irradiation with unfiltered light, the spectrum of the film has a shape typical of bulk metal. At $\lambda_{exc} \geq 365$ nm, the photochemical process finishes on the stage of reduction of Au(III) to Au(I) and of Cu(II) to Cu(I). Reductions of Au(I), Cu(I), and Ag(I) to the zero-valent state fail, since their energy corresponds to the far UV spectral range.

**Concentration of initial complex.** This is the second most important experimental factor influencing the kinetics of photochemical formation of colloids and their dispersity. Increase of the Au(III) and Cu(II) contents in photolytes simultaneously increase the induction period of the process (Fig. 5) and the quantum yield of photocatalytic growth of nanoparticles (Tables 1–3).

The dependences of the particle size on quartz surface on the concentration of the complex are identical for copper and gold and extremal in nature. Taking into account that the reductive ability of colloidal gold and copper particles increases as their size decreases, the observed effect can be related to oxidation of nuclei and small particles in the nearsurface layer by photolyte Au(III) and Cu(II) ions . Increasing concentration of the oxidant [Au(III) and Cu(II)] in the system decreases the lifetime of small particles whose dimensions are smaller than the critical photostable size. As a consequence, the probability of coalescence of such small particles in a process preceding their adsorption on quartz surface decreases.

The particle size of the copper, silver, and gold colloids, obtained in porous quartz and MF-4SK membranes is almost independent of the concentration of the initial complex, which is caused by the fact that nanoparticle growth is restricted by the pore volume.

In homogeneous rigid matrices (glycerin, polyvinyl alcohol, polyethylene glycol, and gelatin) where the particles growth due to coalescence is suppressed by strong diffusion restrictions, varying the concentration of the initial complex is an effective tool for controlling the process. Within the concentration range 0.05–0.25 M, particle size gradually decreases with decreasing concentration.

The role of the **viscosity of the medium, the geometry of the reaction system,** and other influencing factors are illustrated by the example of gold in Fig. 12.

Simple calculations show that the concentration of intermediates, needed for initiation of the process, is

attained, under the experimental conditions (spectral range, light intensity, concentration of light-sensitive complex) used, in a thin (~1 mm) photolyte layer. Thicker working layers (more than 2 mm) are discouraged, leading to diffusion of intermediates to bulk solution and to their fast oxidation [$O_2$, Au(III), Cu(II), Pd(II)]. Deaeration of photolytes partially lifts this restriction and, for example, makes possible working with photocells up to 5 cm in thickness. However, here, too, deposition proceeds, due to photoinduced adsorption, only on a frontal cell wall, i.e. in the region of high intensity of absorption. Increasing photolyte viscosity enhances stability of intermediates and, as a consequence, increases the quantum yield of the process until diffusion comes into forth to limit cluster formation and growth (Table 3). At high contents of glycerol and ethylene glycol or with solid polymers, diffusion of clusters to quartz surface becomes impossible, so that the process proceeds only in photolyte bulk. We used this approach to obtain stable bulk colloidal dispersions.

As was shown before, the composition of the initial complex influences the rate of formation and the properties of the resulting colloids. Reasons for this phenomenon require special investigation.

Thus, varying of experimental factors (energy and intensity of light, concentration and nature of initial complex, geometry of photochemical cell, and photolyte viscosity) is a promising tool for photosynthesis of nanophase systems with preset properties.

## REFERENCES

1. Ravaine, S., Fanucci, G.E., Seip, C.T., Adair, J.N., and Talmah, D.R., *Langmuir*, 1998, vol. 14, no. 3, pp. 708–713.
2. Esumi, K., Suzuki, A., Aihara, N., Usui, K., and Torigoe, K., *Langmuir*, 1998, vol. 14, no. 12, pp. 3157–3159.
3. Loginov, A.V., Gorbunova, V.V., and Boitsova, T.B., *Zh. Obshch. Khim.*, 1997, vol. 67, no. 2, pp. 189–201.
4. Yi, K.C., Mendeta, V.S., Castanares, R.L., Meldrum, F.C., Wu, C., and Fendler, J.H., *J. Phys. Chem.*, 1995, vol. 99, no. 24, pp. 9869–9875.
5. Kobayashi, M. and Sato, H., *Chem. Lett.*, 1993, no. 10, pp. 1659–1662.
6. Torigoe, K. and Esumi, K., *Langmuir*, 1992, vol. 8, no. 1, pp. 59–63.
7. Boitsova, T.B., Loginov, A.V., and Gorbunova, V.V., *Zh. Obshch. Khim.*, 1997, vol. 67, no. 10, pp. 1741–1742.
8. Boitsova, T.B., Loginov, A.V., and Gorbunova, V.V., *Zh. Prikl. Khim.*, 1997, vol. 70, no. 10, pp. 1585–1590.
9. Boitsova, T.B., Loginov, A.V., and Gorbunova, V.V., *Neorg. Mater.*, 1999, vol. 35, no. 12, pp. 1449–1454.
10. Bohren, C.F. and Huffman, D.R., *Absorption and Scattering of Light by Small Particles*, New York: Wiley, 1983.
11. Petrov, Yu.I., *Klastery i malye chastitsy* (Clusters and Small Particles), Moscow: Nauka, 1986.
12. Henglein, A., *J. Phys. Chem.*, 1993, vol. 97, no. 21, pp. 5457–5471.
13. Boitsova, T.B., Gorbunova, V.V., and Loginov, A.V., *Zh. Obshch. Khim.*, 1999, vol. 69, no. 12, pp. 1937–1943.
14. Gorbunova, V.V., Voronin, Yu.M., and Boitsova, T.B., *Opt. Zh.*, 2001, vol. 68, no. 10, pp. 1746–1751.
15. *Khimicheskoe osazhdenie metallov iz vodnykh rastvorov* (Chemical Deposition of Metals from Aqueous Solutions), Sviridov, V.V., Ed., Minsk: Belorus. Univ., 1987.